European Journal of Pharmaceutics and Biopharmaceutics 80 (2012) 306–314

Contents lists available at SciVerse ScienceDirect

European Journal of Pharmaceutics and Biopharmaceutics

journal homepage: www.elsevier.com/locate/ejpb

Research paper

Nanoparticulate lipid dispersions for bromocriptine delivery: Characterization and in vivo study

Elisabetta Esposito [a,*], Paolo Mariani [b], Laura Ravani [a], Catia Contado [c], Mattia Volta [d], Simone Bido [d], Markus Drechsler [e], Serena Mazzoni [b], Enea Menegatti [a], Michele Morari [d], Rita Cortesi [a]

[a] Department of Pharmaceutical Sciences, University of Ferrara, Ferrara, Italy
[b] SAIFET Department, Università Politecnica delle Marche, Ancona, Italy
[c] Department of Chemistry, University of Ferrara, Ferrara, Italy
[d] Department of Experimental and Clinical Medicine, University of Ferrara, Ferrara, Italy
[e] Macromolecular Chemistry II, University of Bayreuth, Germany

ARTICLE INFO

Article history:
Received 10 December 2010
Accepted in revised form 22 October 2011
Available online 28 October 2011

Keywords:
Solid Lipid Nanoparticles (SLNs)
Nanostructured Lipid Carrier (NLC)
Bromocriptine (BC)
X-ray
Drag test
Bar test

ABSTRACT

The physico-chemical properties and in vivo efficacies of two nanoparticulate systems delivering the antiparkinsonian drug bromocriptine (BC) were compared in the present study. Monoolein Aqueous Dispersions (MADs) and Nanostructured Lipid Carriers (NLCs) were produced and characterized. Cryogenic transmission electron microscopy (cryo-TEM) and X-ray diffraction revealed the morphology of MAD and NLC. Dimensional distribution was determined by Photon Correlation Spectroscopy (PCS) and Sedimentation Field Flow Fractionation (SdFFF). In particular, BC was shown to be encapsulated with high entrapment efficiency both in MAD and in NLC, according to SdFFF combined with HPLC. Two behavioral tests specific for akinesia (bar test) or akinesia/bradykinesia (drag test) were used to compare the effects of the different BC formulations on motor disabilities in 6-hydroxydopamine hemilesioned rats in vivo, a model of Parkinson's disease. Both free BC and BC–NLC reduced the immobility time in the bar test and enhanced the number of steps in the drag test, although the effects of encapsulated BC were longer lasting (5 h). Conversely, BC–MAD was ineffective in the bar test and improved stepping activity in the drag test to a much lower degree than those achieved with the other preparations. We conclude that MAD and NLC can encapsulate BC, although only NLC provide long-lasting therapeutic effects possibly extending BC half-life in vivo.

1. Introduction

Lipid dispersions have attracted significant attention due to their potential use as matrixes able to dissolve and deliver active molecules in a controlled fashion, thereby improving their bioavailability and reducing side-effects [1,2].

Solid Lipid Nanoparticles (SLNs) are delivery systems in which the nanodispersed phase has a solid matrix of crystalline solid lipids. SLN are able to protect encapsulated molecules from degradation and modulate their release [3]. The second generation of SLN is represented by Nanostructured Lipid Carriers (NLCs), which are composed of a solid lipid matrix with a certain content of a liquid lipid phase [4]. For instance, the mixture of caprylic/capric triglycerides (liquid at room temperature) with a solid lipid such as tristearin leads to the formation of solid carriers with homogenous lipid nanocompartments [5].

Another type of lipid dispersion that can provide matrices for the sustained release of drugs is represented by Monoolein Aqueous Dispersions (MADs).

The self-assembly of amphiphilic lipids such as monoglycerides in water gives rise to complex lyotropic liquid crystalline nanostructures like micellar, lamellar, hexagonal, and cubic phases [1,6]. The predominance of one species over the other mainly depends on temperature and water content of the system [7].

Cubosomes can be defined as stable reverse bicontinuous structures with two distinct regions of water separated by a contorted bilayer [8]. The methods of preparation [9,10] and the inner structure [11,12] of cubosomes have been widely studied. Nevertheless, drug release from these systems has been poorly investigated [13].

The use of lipid nanosystems for the therapy of brain diseases has been recently proposed [14,15]. Indeed, the pharmacological

Abbreviations: MADs, Monoolein aqueous dispersions; PSD, particle size distribution.

* Corresponding author. Dipartimento di Scienze Farmaceutiche, Via Fossato di Mortara, 19, I-44100 Ferrara, Italy. Tel.: +39 532 455259; fax: +39 532 291296.
E-mail address: ese@unife.it (E. Esposito).

0939-6411/$ - see front matter © 2011 Elsevier B.V. All rights reserved.
doi:10.1016/j.ejpb.2011.10.015

treatment of brain tumors, as well as neurological and psychiatric disorders, is often hindered by the inability of potent drugs to pass the blood brain barrier (BBB) [16]. BBB significantly restricts water-soluble, charged and high molecular weight therapeutics to the vascular space, while allowing brain penetration of small and/or lipophilic molecules. Multiple strategies have been employed to circumvent BBB. An emerging approach is the use of colloidal carriers, which allow brain penetration of non-transportable drugs by masking their physico-chemical characteristics [17,18]. In fact, colloidal carriers represent a non-invasive mean of administration, which offers clinical advantages such as the reduction in drug dosage and side-effects, the increase in drug viability, and the improvement of patient quality of life [19].

In a recent study, we demonstrated the potential application of NLC as a delivery system of the dopamine receptor agonist bromocriptine (BC) for Parkinson's disease (PD) therapy [20]. This follow-up study was aimed at investigating the use of MAD as formulations for controlled delivery of BC. An in-depth characterization of morphology, size, inner structure, and drug distribution of NLC and MAD was made. In addition, the ability of both BC preparations to attenuate motor deficits in 6-hydroxydopamine (6-OHDA) hemilesioned rats, a model of PD, was determined in vivo and compared to that of free BC.

2. Materials and methods

2.1. Materials

RYLO MG 19, glyceryl monooleate (MO) was a gift from Danisco Cultor (Grindsted, Denmark). Pluronic F127 (PEO_{98}–POP_{67}–PEO_{98}) (poloxamer 407) was obtained from BASF (Ludwigshafen, Germany).

Lutrol F 68, oxirane, methyl-, polymer with oxirane (75;30) (poloxamer 188) was a gift of BASF ChemTrade GmbH (Burgbernheim, Germany). FL-70 is a detergent (water 88.8%, triethanolamine oleate 3.8%, sodium carbonate 2.7%, alcohols, C12-14-secondary, ethoxylated 1.8%, tetrasodium ethylenediaminetetraacetate 1.4%, Polyethylene glycol 0.9%, sodium oleate 0.5%, sodium bicarbonate 0.1%) and was obtained from Fisher Scientific (Fair Lawn, NJ, USA) [21].

Tristearin, stearic triglyceride (tristearin), was provided by Fluka (Buchs, Switzerland). Miglyol 812, caprylic/capric triglycerides (Miglyol), was purchased from Eigenmann & Veronelli (Rho, Milano, Italy).

Bromocriptine mesylate, 2-Bromo-α-ergocriptine methansulfonate salt (BC), amphetamine, and 6-hydroxydopamine (6-OHDA) were purchased from Sigma Chemical Company (St Louis, MO, USA).

2.2. MAD preparation

Production of dispersions was based on the emulsification of MO (4.5% w/w) and poloxamer 407 (0.5% w/w) in water (95% w/w), as described by Esposito et al. [22]. After emulsification, the dispersion was subjected to homogenization (15,000 rev min^{-1}, Ultra Turrax, Janke & Kunkel, Ika-Werk, Sardo, Italy) at 60 °C for 1 min, then cooled and maintained at room temperature in glass vials.

Twelve point five (12.5) milligrams of BC (0.55% w/w with respect to the monoolein, 0.025% w/w with respect to the dispersion) was added to the molten MO/poloxamer solution and dissolved before addition to the aqueous solution.

A representative amount of dispersion was analyzed by cryo-TEM. The dispersion was then filtered through a mixed esters cellulose membrane (1.2 μm pore size) to separate large MO/poloxamer aggregates. Dimensional characterization of MO dispersions as well as in vivo experiments was performed after filtration.

The density of MAD (0.0133 g/ml) was calculated as reported in Supplementary data.

2.3. NLC preparation

NLC were prepared by stirring followed by ultrasonication [20]. Briefly, 1 g of lipid mixture was melted at 75 °C. The lipid mixture was constituted of tristearin/Miglyol 2:1 w/w. The fused lipid phase was dispersed in 19 ml of an aqueous poloxamer 188 solution (2.5% w/w). The emulsion was subjected to ultrasonication (Microson™, Ultrasonic cell Disruptor) at 6.75 kHz for 15 min and then cooled down to room temperature by placing it in a water bath at 22 °C. NLC dispersions were stored at room temperature.

Five milligrams of BC (0.025% w/w with respect to the total dispersions, 0.5% w/w with respect to the lipid phase) was added to the molten lipid mixture and dissolved before addition to the aqueous solution. The density of NLC (0.0283 g/ml) was obtained as described for MAD in Supplementary data.

2.4. Characterization of lipid dispersions

Water and disperse phase loss after dispersion production were determined as reported in Supplementary data.

2.4.1. Photon Correlation Spectroscopy (PCS)

Submicron particle size analysis was performed using a Zetasizer 3000 PCS (Malvern Instr., Malvern, England) equipped with a 5 mW helium neon laser with a wavelength output of 633 nm. The dispersant refractive index was 1.33 and the absorbance was 0.00. Glassware was cleaned of dust by washing with detergent and rinsing twice with sterile water. Measurements were made at 25 °C at an angle of 90° with a run time of at least 180 s. Samples were diluted with bidistilled water in a 1:10 V:V ratio. Data were analyzed using the "CONTIN" method [23].

2.4.2. Sedimentation Field Flow Fractionation Analysis

A Sedimentation Field Flow Fractionation (SdFFF) system (Model S101, FFFractionation, Inc., Salt Lake City, UT, USA), described elsewhere [24], was employed to determine the size distribution of particles (PSD) by converting the fractograms, i.e., the graphical results, assuming the particle density is known [25]. The mobile phase was a 0.01% v/v solution of FL-70 in Milli-Q water (Millipore S.p.A., Vimodrone, Milan, Italy) pumped at 2.0 ml/min and monitored in each run. Fifty microliter samples were injected as they were through a 50 μl Rheodyne loop valve.

The fractions were automatically collected by a Model 2110 fraction collector positioned at the end of the SdFFF system (Bio Rad laboratories, UK) after setting a collecting time of 90 s. The volume of each fraction was 3 ml.

2.4.3. Cryogenic Transmission Electron Microscopy (Cryo-TEM)

Samples were vitrified as described in a previous study by Esposito et al. [9]. The vitrified specimen was transferred to a Zeiss EM922Omega (Zeiss SMT, Oberkochen, Germany) transmission electron microscope using a cryoholder (CT3500, Gatan, Munich, Germany). Sample temperature was kept below 100 K throughout the examination. Specimens were examined with doses of about 1000–2000 e/nm^2 at 200 kV. Images were recorded by a CCD digital camera (Ultrascan 1000, Gatan) and analyzed using a GMS 1.8 software (Gatan).

2.4.4. X-ray diffraction measurements

Low-angle X-ray scattering experiments were performed at the DESY synchrotron facility on the A2 beamline in Hamburg, Germany. The investigated Q-range ($Q = 4\pi \sin\theta/\lambda$, where 2θ is the scattering angle and $\lambda = 1.50$ Å the X-ray wavelength) was

0.02–0.35 $Å^{-1}$. Experiments were performed in the 20–40 °C range. Scattering data were recorded on a bidimensional CCD camera of 1024 × 1024 pixels, radially averaged and corrected for the dark, detector efficiency and sample transmission [26]. A few wide-angle X-ray diffraction experiments were performed using a laboratory 3.5 kW Philips PW 1830 X-ray generator equipped with a Guinier-type focusing camera operating with a bent quartz crystal monochromator (λ = 1.54 Å). Diffraction patterns were recorded on GNR Analytical Instruments Imaging Plate system. Samples were held in a tight vacuum cylindrical cell provided with thin Mylar windows. Diffraction data were collected at 20 °C.

In each experiment, a number of Bragg peaks were detected in the low-angle X-ray diffraction region. The peak indexing was performed considering the different symmetries commonly observed in lipid phases [27]. From the averaged spacing of the observed peaks, the unit cell dimension, *a*, was calculated using the Bragg law. The nature of the short-range lipid conformation was derived analyzing the high-angle X-ray diffraction profiles [28].

2.5. Drug content of dispersions

The method used to determine BC content in the dispersion is reported in Supplementary data. BC associated with particles was quantified by HPLC analyses of several fractions collected after the separation by SdFFF.

2.6. HPLC procedure

HPLC determinations were performed using a two-plungers alternative pump (Jasco, Japan), an UV-detector operating at 305 nm, and a 7125 Rheodyne injection valve with a 50 µl loop. Samples were loaded on a stainless steel C-18 reverse-phase column (15 × 0.46 cm) packed with 5 µm particles (Hypersil BDS, Alltech, USA).

Elution was performed with a mobile phase containing 0.1 M ammonium formate (pH 3) and acetonitrile 55:45 v/v at a flow rate of 0.8 ml/min. Retention time of BC was 5.8 min [20].

2.7. In vivo tests

Male Sprague-Dawley rats were kept under regular lighting conditions (12 h light/dark cycle) and given food and water ad libitum. The experimental protocols used in the present study were approved by the Italian Ministry of Health (license n. 194/2008-B) and by the Ethical Committee of the University of Ferrara. Adequate measures were taken to minimize animal pain and discomfort and to limit the number of animals employed in the study.

2.7.1. 6-Hydroxydopamine lesion

Unilateral lesion of dopamine (DA) neurons was induced in isoflurane-anaesthetized male Sprague-Dawley rats (150 g; Harlan Italy; S. Pietro al Natisone, Italy) as previously described [29]. Eight micrograms of 6-OHDA, dissolved in 4 µl of saline (NaCl 0.9% w/v) containing 0.02% ascorbic acid, was stereotaxically injected according to the following coordinates from bregma: antero-posterior – 4.4 mm, medio-lateral – 1.2 mm, dorso-ventral – 7.8 mm below dura [30]. In order to select the rats that had been successfully lesioned, the rotational model was employed. Two weeks after 6-OHDA injection, rats were tested for denervation with a dose of amphetamine (5 mg/kg i.p., dissolved in saline). Forty-nine rats showing a turning behavior >7 turns/min in a direction ipsilateral to the lesion side were enrolled in the study. Experiments were usually performed 6–8 weeks after lesion. Marked (>95%) reduction in striatal DA levels and tyrosine hydroxylase-positive DA terminals have been detected at this stage [31,32].

2.7.2. Behavioral studies in hemiparkinsonian rats

The 6-OHDA hemilesioned rat is a well-established model of experimental parkinsonism, in which hypokinetic motor disturbance primarily affects the side of the body contralateral to the denervated hemisphere (i.e., the toxin injection side). Parkinsonian-like disabilities were investigated in rats by using two previously validated behavioral tests [30,32]. The "bar test" measures the ability of the rat to respond to an externally imposed static posture and provides information on the time to initiate a movement (akinesia) [33]. The "drag test" measures the ability of the forepaws to adapt to an external dynamic stimulus (i.e., dragging backwards) and provides information on the time to initiate and execute (bradykinesia) a movement [29,34].

In the bar test, the contralateral and ipsilateral forepaws of each rat were alternatively placed on blocks of increasing heights (3, 6, and 9 cm). The immobility time (in seconds) of each paw on the blocks was recorded (cut-off time at each step of 20 s) and summed. In the drag test, the animal was gently lifted from the tail, allowing the forepaws to rest on the table, and dragged backwards at a constant speed (20 cm/s) for 100 cm. The adjusting steps made with the forepaws were counted by two distinct observers. Rats were trained on both motor tasks until their performance was reproducible. On the day of experiment, motor performance in the bar and drag test was evaluated before (control session) and at different time-points after drug administration (30, 90, 180, 300, 480 min). Drug effect has been expressed as a percent of pre-treatment values. BC preparations (free BC, BC–MAD, and BC–NLC) were given intraperitoneally (i.p.) at a dose of 0.3 mg/Kg (9–13 animals each group). Free BC was administered in a saline solution (0.9 mg/ml). The effect of vehicle (empty MAD and empty NLC) was also investigated (7–9 animals each group). The dose of the lipid given to each rat was calculated to be 70 mg/Kg and 67 mg/Kg for NLC and MAD, respectively.

2.7.3. Statistical analysis

Statistical analysis was performed on percent data by one-way repeated measures (RM) analysis of variance (ANOVA). In case ANOVA yielded to a significant *F* score, post hoc analysis was performed by contrast analysis to determine group differences. In case a significant time × treatment interaction was found, the sequentially rejective Bonferroni's test was used (implemented on excel spreadsheet) to determine specific differences (i.e., at the single time point level) between groups. p-Values < 0.05 were considered to be statistically significant.

3. Results and discussion

For several years, we have been trying to develop an approach to deliver BC in a controlled fashion [35,36]. Our interest in this molecule arises from its wide therapeutic potential. BC is a dopamine receptor agonist used for the treatment of pituitary tumors, PD, hyperprolactinaemia, neuroleptic malignant syndrome, and recently approved for the treatment of type 2 diabetes [37].

We previously produced and characterized SLN to deliver BC, demonstrating that NLC constituted of tristearin/Miglyol mixture can prolong BC antiparkinsonian action in vivo [20]. In the present study, we investigated MAD as an alternative nanotechnology system to deliver BC. MAD are biocompatible nanosystems able to incorporate lipid molecules in a molecular sponge consisting of interpenetrating nanochannels filled with water and coated by lipid bilayers [38]. Much interest grew around cubic phases because of their unique biologically compatible microstructure, which is capable to control the release of soluble molecules such as drugs and proteins [39]. Like NLC, MAD represents an interesting alterna-

tive to liposomes, being characterized by a higher viscous resistance to rupture and a consequent greater stability.

3.1. Characterization of dispersions

Table 1 summarizes the results of PCS studies conducted to determine the dimensional distribution of MAD and NLC dispersions, in the absence and in the presence of BC.

Both MAD and NLC had mean intensity diameters of ~200 nm. Empty MAD had a mean diameter of 198.2 nm, expressed as Z Average. The analysis by volume revealed a mean diameter of 121.0 nm. BC incorporation slightly increased the mean diameter of nanostructures to 204.8 nm. In-depth analysis of the distribution by volume revealed a huge peak with a mean diameter of 109.1 nm (84.3% of Peak Area) and a smaller one with a mean diameter of 286.3 nm (15.7%). After filtration, the mean size of the larger particles measured by laser diffraction was 28 ± 2.7 μm (mean ± SD of three runs), ranging between 25 and 30 μm (data not shown).

NLC dispersions were not filtered since they did not display aggregates or large microparticles. Empty NLC showed a mean diameter of 196.2 nm, which was not affected by BC incorporation, even if the amount of larger nanoparticles increased, conferring the distribution a bimodal profile. Dimensional analysis by volume revealed a mean diameter of 131.4 nm for the more conspicuous population and a mean diameter of 392.4 nm for the other. On the other hand both populations displayed low polydispersity indexes (0.18 and 0.19), indicating a narrow dimensional distribution [22].

Size distribution was also determined by SdFFF. The fractograms obtained under the same separation conditions (to allow a direct comparison) were converted into PSD plots, i.e., the amount of material per unit change of diameter, according to well-proven equations, by transforming the retention time in the diameter of the equivalent sphere (d), and the UV signal into a mass frequency function (dd) [24,40]. Fig. 1 shows the PSD plots of a diluted amount of BC–MAD (panel A) and BC–NLC (panel B) dispersions. The conversion was performed by assuming an average density of 0.0133 g/ml for MAD and 0.0283 g/ml for NLC. In panel A, the main peak had a maximum at ~130 nm and showed a small shoulder, possibly masking a minor population of particles of ~160 nm size, as also evidenced in the original fractogram reported in the inset of panel A. These size distributions partly differed from PCS data reported in Table 1. However, the cryo-TEM image reported below (Fig. 2) confirms the presence of particles of different size, structure, and possibly density, which generates particle masses difficult to be efficiently separated under these experimental conditions.

As shown in a previous study [20], NLC particles had instead a quite regular and reproducible shape, independent of their size, thus also their density might be considered constant, guaranteeing a better reliability to the SdFFF results presented in panel B. The graph shows a thin peak centered at ~100 nm and another one, smaller and broader, with a maximum at ~275 nm. These data are in good agreement with the PCS analysis. The apparent

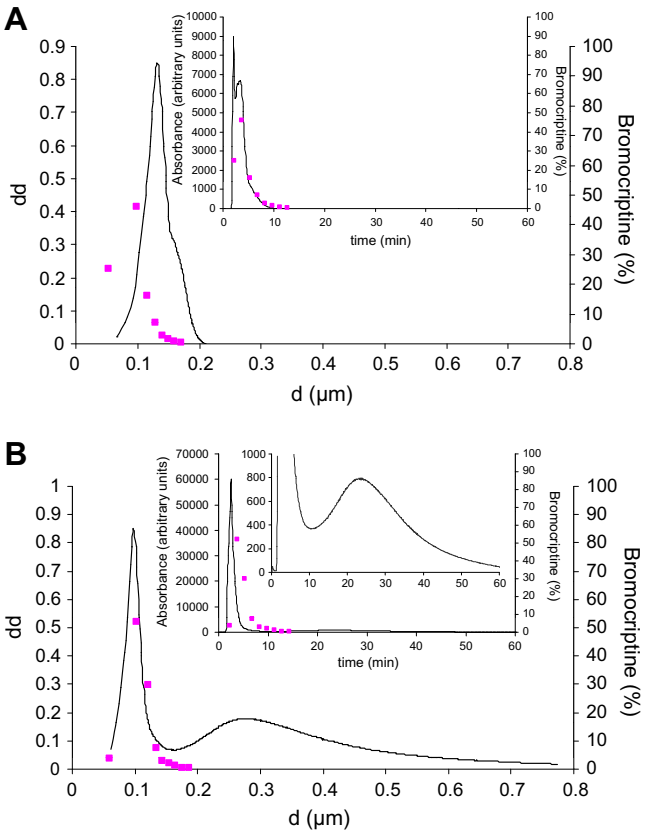

Fig. 1. PSDs elaborated from the SdFFF fractograms. (A) MAD particles were assumed to have a density of 0.0133 g/ml (d = diameter of nanoparticles; dd = dimensional distribution; the dots indicate BC content, as determined by HPLC). (B) NLC particles: assumed density 0.0283 g/ml. (For interpretation of the references to color in this figure legend, the reader is referred to the web version of this article.)

discrepancy in the relative proportions between the two peaks is an artifact introduced by the conversion into PSD, as it can be verified by observing the original fractogram reported on the top of panel B, where the larger peak is scarcely visible from the baseline, unless to zoom in the graph.

Cryo-TEM analyses were conducted in order to investigate the internal structures of MAD and NLC. Fig. 2 reports cryo-TEM images of a sample of non-filtered BC–MAD. Well-shaped particles with a homogeneous, ordered inner structure can be observed. Upon closer inspection, images reveal two different internal patterns (labeled C and H), with a predominance of the C over the H structural motif (panel A). The H motif also appears in some larger particles (panel B) with poly-"crystalline" nature, whereas smaller particles show a single internal structure. Finally, particles with ordered inner structure and vesicular structures attached on their surface can be observed, as previously found by other authors [7].

Fast Fourier transform (FFT) analysis was used to characterize the internal morphology of the particles, since FFT easily allows

Table 1
Mean diameters of MAD and NLC determined by PCS.

Parameter	MAD dispersion	BC–MAD dispersion[a]	NLC dispersion	BC–NLC dispersion[a]
Z Average mean diameter (nm)	198.2 ± 1.2	204.8 ± 1.2	196.2 ± 2.4	195.1 ± 3.3
Analysis by volume mean diameter (nm)	121 ± 2.5 (Peak Area 100%)	109.1 ± 2.4 (Peak Area 84.3 ± 3.2%) 286.3 ± 3.3 (Peak Area 15.7 ± 4.1%)	135.9 ± 3.2 (Peak Area 100%)	101.4 ± 1.8 (Peak Area 85.5 ± 3.1%) 272.4 ± 2.2 (Peak Area 14.5 ± 2.3%)
Polydispersity index	0.18 ± 0.02	0.19 ± 0.01	0.18 ± 0.02	0.19 ± 0.03

PCS data are means of five determinations on different batches of the same type of dispersion.
[a] Produced in the presence of bromocriptine.

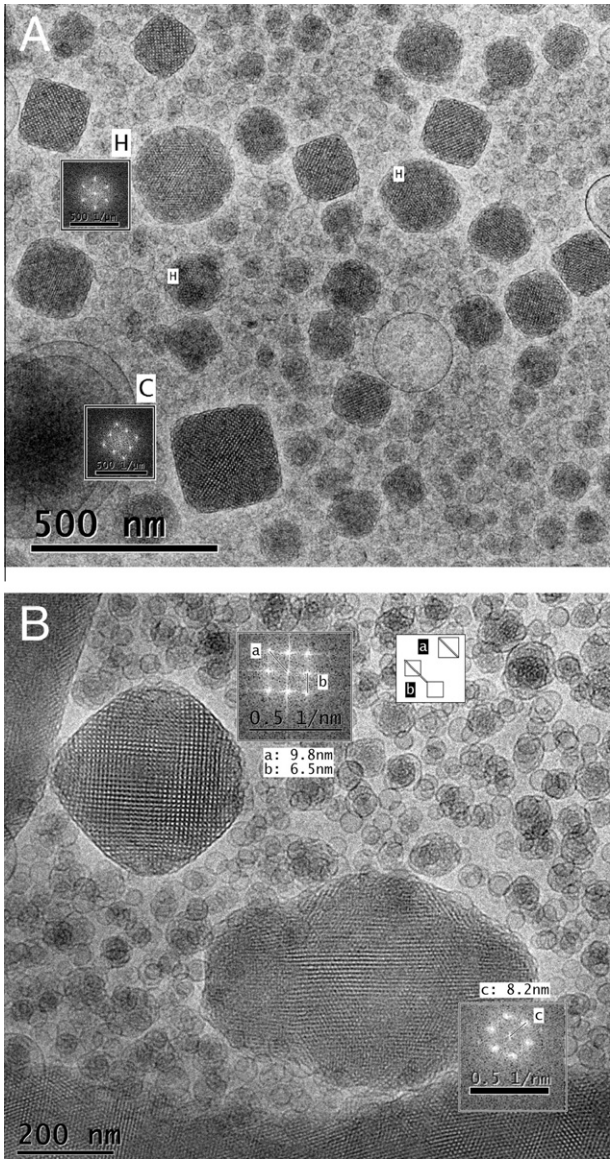

Fig. 2. Cryo-TEM images of BC–MAD. The insets show Fast Fourier transforms of some particles.

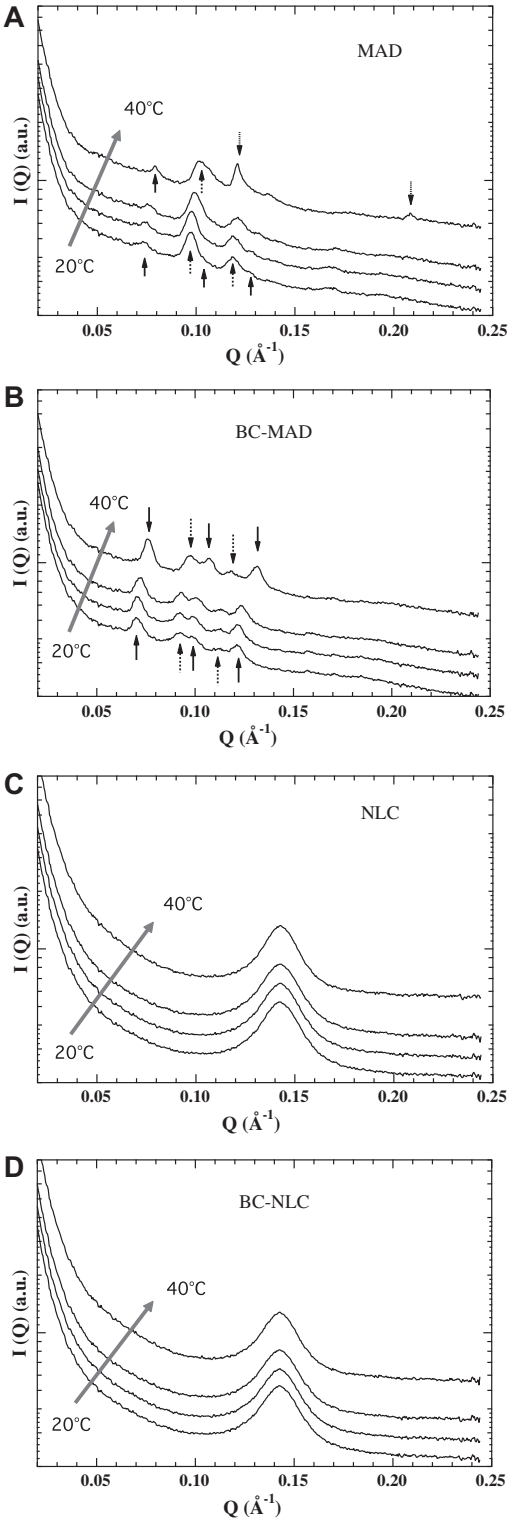

Fig. 3. Low-angle X-ray diffraction profiles observed from MAD and NLC samples at different temperatures. Measurements have been performed at 20, 25, 30, and 40 °C, scattering curves are stacked consistently, following the direction of the gray arrows. In panels A and B, small arrows indicate the peak indexing: upward, continuous arrow, *Im3m* phase (the indicated peak sequence is [110], [200], [211]); upward, dashed arrow, *Pn3m* phase ([110] and [111]); downward, pointed arrow, *H* phase ([10] and [21]).

to obtain an optical diffractogram similar to an electron diffraction pattern. In this way, periodic or repeatable distances in the mesophase structure could be detected, together with the symmetry of the motif. According to the different internal morphologies shown in Fig. 2, FFT evidenced two different patterns. The first, observed in the particles with the H structural motif, corresponds to a two dimensional (2D) hexagonal symmetry with 2D lattice parameters $v = w = 8.2$ nm (labeled c in panel B) and $\gamma = 120°$. The second, observed in the particles with the C structural motif, corresponds to a rectangular symmetry with 2D lattice parameters $v = 6.5$ nm (labeled a), $w = 9.8$ nm (labeled b), and $\gamma = 90°$.

The presence of particles with two different inner structures was also indicated by X-ray diffraction results. However, since both structures are cubic, data definitely prove that MAD dispersions are cubosomes. Fig. 3 (panels A and B) shows the low-angle X-ray diffraction profiles of empty and BC–MAD obtained as a function of temperature. At room temperature, diffraction profiles are characterized by two series of peaks, consistent with the presence of dispersed cubic phase particles of *Pn3m* and *Im3m* symmetry. In other words, in the presence and in the absence of BC, MAD dispersions can exhibit D-type or P-type structures. Phase coexistence in the MO/poloxamer 407/water disperse system has already been

Table 2
Structure identifications and unit cell dimensions observed in the different samples at various temperatures.

Sample	Temp. (°C)	Phase and unit cell (nm)						Hydrocarbon chain conformation
MAD	20	Im3m	12.11	**Pn3m**	9.16			α
	25	Im3m	12.01	**Pn3m**	9.11			α
	30	Im3m	11.77	**Pn3m**	8.99			α
	40	Im3m	11.25	**Pn3m**	8.71	H	6.01	α
BC-MAD	20	**Im3m**	12.69	Pn3m	9.66			α
	25	**Im3m**	12.64	Pn3m	9.65			α
	30	**Im3m**	12.41	Pn3m	9.58			α
	40	**Im3m**	11.72	Pn3m	9.14			α
NLC	20–40[a]	L	4.42					β
BC-NLC	20–40[a]	L	4.42					β

When samples show more than one structure, the one characterized by the higher X-ray diffraction profile is shown in bold. Error in unit cells is ±0.02 nm.
[a] From 20 to 40° C, i.e., 20, 25, 30, and 40 °C.

observed [11], even if in the same conditions the presence of a pure *Im3m* phase was also reported [8]. As previously discussed [41], the different structural behaviors of MAD may be related to differences in composition (e.g., MO quality, buffer, ionic force of the aqueous solution) and production procedures (e.g., ultrasonication, homogenization, temperature and pressure parameters). However, the present results confirmed that at this poloxamer 407 concentration, the cubic and not the vesicular structure is the equilibrium state, even in the presence of BC. It should be noticed that both types of cubic structures detected in our preparation are bicontinuous, but the P-surface structure only occurs in the MO–water system when a third component is added [42]. Moreover, the lattice constants, which have been derived from peak positions (Table 2), are very similar to those reported by Nakano et al. [11]. More interestingly, lattice constants are slightly sensitive to the presence of BC, probably due to an increased hydration of the lipid phases induced by BC.

Cryo-TEM and X-ray diffraction results are in perfect agreement. Indeed, the FFT patterns suggest that the H and C structural motifs correspond to planes normal to the crystallographic directions [1 1 1] and [1 1 0] of a cubic lattice, respectively (Fig. 2). Concerning the H motif, it should be recalled that the projection of a 3D cubic array on 2D is hexagonal when visualized along the [1 1 1] direction and that the corresponding 2D lattice parameters are related to the cubic unit cell dimension a by $v = w = a/\sqrt{2}$. This does neither allow to identify the space group of the particle internal structure nor to differentiate between a hexagonal and a cubic structure. However, the comparison of 2D lattice values with the unit cell dimensions determined by X-ray diffraction (Table 2) strongly suggests that the H particles are cubosomes with an inner cubic structure belonging to the *Im3m* space group. It is worthy of mention that only the *Pn3m* and *Im3m* space groups are allowed in cubosome dispersions because those are the only two space groups established in reversed bicontinuous cubic phases in excess water [43] or in reversed bicontinuous cubic phase dispersions [12]. Concerning the C-motif, the observed 2D lattice parameters are consistent with the ideal values for a cubic array ($v = w/\sqrt{2}$) and correspond to a cubic unit cell dimension a of 9.8 nm. This value compares well with the unit cell of the *Pn3m* cubic phase determined in the same system by X-ray diffraction (Table 2), indicating that C particles are cubosomes with an inner cubic structure belonging to the *Pn3m* space group. Overall, cryo-TEM images of BC–MAD dispersed particles gave strong and direct evidence for the coexistence of cubosomes with two different internal structures: one with a *Pn3m* space group and a lattice parameter of 9.8 nm and another with *Im3m* space group and a lattice parameter of 11.6 nm.

X-ray diffraction experiments also reveal the thermal stability of MAD. As shown in Fig. 3, both D- and P-type cubosomes exist at all the investigated temperatures. However, in empty MAD samples, two other peaks, characteristic of a 2D hexagonal space group, appeared at 40 °C. Since at this temperature, the peaks of the *Pn3m* cubic structure broadened, it appears that temperature induces a D-type cubosome-to-hexasome phase transition [12,44]. Therefore, even if the inner structure of MAD can be highly dependent on manufacturing parameters and then be relevant for the properties of the dispersions, X-ray diffraction demonstrates that the presence of D-type cubosomes does not cause the complete loss of the cubic state of the particles at relatively high temperatures.

Empty and BC–NLC dispersions have been already characterized [20]. In addition, low-angle X-ray diffraction obtained as a function of temperature is now reported (see Fig. 3, panels C and D). In agreement with previous observation [20], both in the absence and in the presence of BC, the diffraction profile is characterized by a large peak, whose position is unaffected by temperature and BC addition (Table 2). The inner lamellar order and the strong structural stability of NLC, even in the presence of BC, appear also confirmed.

3.2. BC encapsulation

HPLC analyses revealed that BC recovery after the production process in the filtered dispersion was 70 ± 0.75% (MAD) and 84 ± 0.58% (NLC) of the total amount of drug used for the preparation. The values of drug loss were taken in consideration to determine BC encapsulation.

SdFFF was employed to obtain information about the drug distribution in the dispersions. During the fractionation, some fractions were collected and analyzed by HPLC to quantify the amount of drug contained in the different particle populations of the disperse phase. In Fig. 1, the concentration of BC determined by HPLC is reported. BC was found to be entirely associated with particles in both MAD and NLC dispersions.

The fraction corresponding to a mean diameter of about 54 nm contains 25% of the total drug, as shown in panel A. The highest amount of BC (46%) is contained in the most representative portion of nanoparticles/vesicles, having a diameter of 98 nm. The remaining 29% of BC is associated with the least representative population of particles, having larger diameters. In fact, cryo-TEM and PCS analyses showed that MAD are mainly characterized by vesicles and cubosomes with 90–100 nm mean diameter, and few structures with larger dimensions.

Also for NLC, whose PSD is reported in panel B, the highest amount of BC (52%) is contained in the most representative fraction, characterized by particles with a mean diameter of ~103 nm. The fraction corresponding to a mean diameter of ~59 nm contains only 3.5% of the total drug, the remaining 44.5% of BC being found into a less representative population of larger particles.

3.3. In vivo tests

In 6-OHDA hemilesioned rats, motor impairment mainly affects the side of the body contralateral to the denervated hemisphere (i.e., the toxin injection side). Consistently, the immobility time of the ipsilateral paw (35.7 ± 1.9 s; $n = 42$) was lower compared to that of the contralateral (parkinsonian) one (47.4 ± 1.9, $n = 42$). Moreover, the number of steps made by the ipsilateral paw was higher (11.1 ± 0.4; $n = 46$) than that made by the contralateral one (1.9 ± 0.1; $n = 46$).

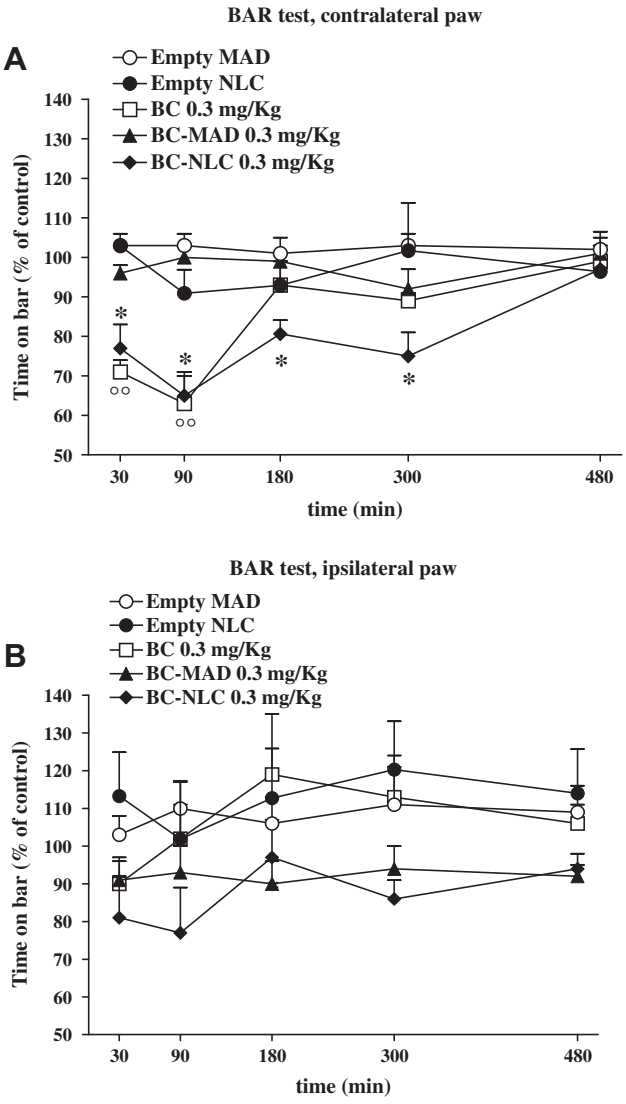

Fig. 4. Systemic administration via i.p. of free bromocriptine (BC) and bromocriptine encapsulated in MAD (BC–MAD) or nanoparticles (BC–NLC) in hemiparkinsonian rats attenuated akinesia in the bar test. The administered dose of BC was always 0.3 mg/Kg. Rats injected with vehicles (empty MAD or NLC) are also shown. Immobility time was calculated at different time-points (30, 90, 180, 300, and 480 min from injection) both at the contralateral (panel A) and at ipsilateral (panel B) forepaw (in sec), and expressed as percent of pre-treatment values. Data are means ± SEM of 7–11 animals per group. $^{**}p < 0.01$ different from empty NLC. $^{\circ\circ}p < 0.01$ different from empty MAD and NLC.

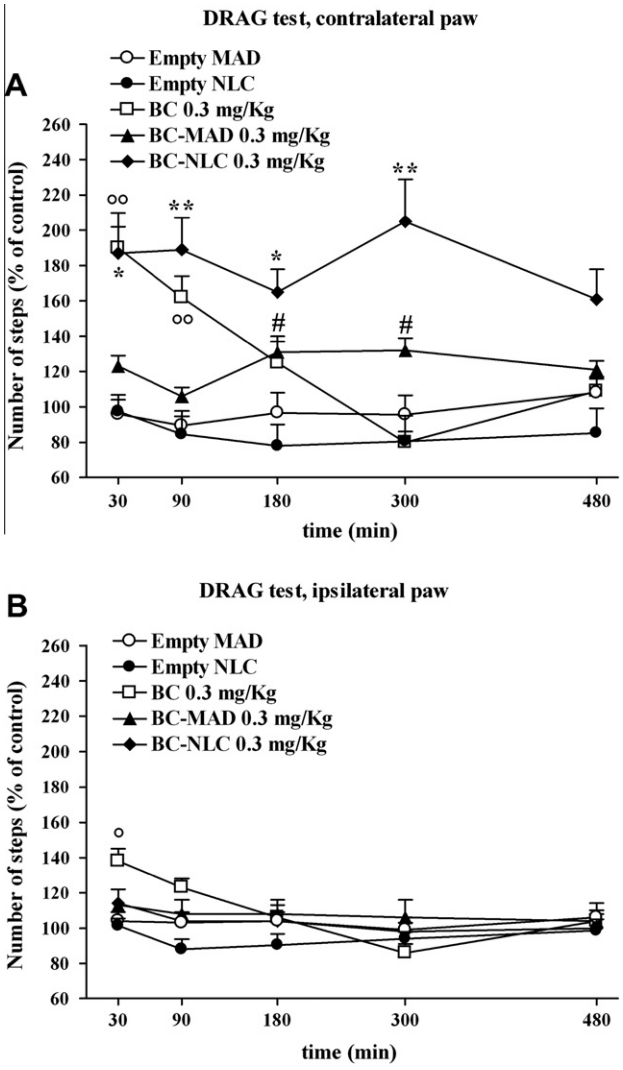

Fig. 5. Systemic administration via i.p. of free bromocriptine (BC) and bromocriptine encapsulated in MAD (BC–MAD) or nanoparticles (BC–NLC) in hemiparkinsonian rats attenuated akinesia/bradykinesia in the drag test. The administered dose of BC was always 0.3 mg/Kg. Rats injected with vehicles (empty MAD or NLC) are also shown. The number of steps was calculated at different time-points (30, 90, 180, 300, and 480 min from injection) both at the contralateral (panel A) and at the ipsilateral (panel B) forepaw, and expressed as percent of pre-treatment values. Data are means ± SEM of 7–13 animals per group. $^{*}p < 0.05$; $^{**}p < 0.01$ different from empty NLC. $^{\circ\circ}p < 0.01$ different from empty MAD and NLC. $^{\#}p < 0.05$ different from empty MAD.

Repeated measure ANOVA on the immobility time at the contralateral paw in the bar test (Fig 4A) revealed main effects of treatment ($F_{4,36} = 15.83$, $p < 0.0001$) and time ($F_{4,155} = 7.51$, $p < 0.0001$), and a time × treatment interaction ($F_{16,155} = 3.58$, $p < 0.0001$). Post hoc analysis showed that both free BC and BC–NLC reduced the time spent on bar (i.e., attenuated akinesia) compared to vehicle-treated animals, although the action of BC–NLC was more prolonged (Fig. 4A). Indeed, both free BC and BC–NLC produced a significant reduction in akinesia 30 min after administration (∼77% and ∼71% of control, respectively) and were maximally effective after 90 min (∼63% and ∼65% of control, respectively). However, the effect of free BC was not significant after 3 h (∼93%) whereas that of BC–NLC was still detectable up to 3 h after administration (∼80%). No significant changes of the immobility time at the ipsilateral paw were induced by any BC formulations (Fig 4B).

Repeated measure ANOVA on the number of steps at the contralateral paw in the drag test (Fig 5A) revealed main effects of treatment ($F_{4,36} = 41.31$, $p < 0.0001$) and time ($F_{4,185} = 3.38$, $p = 0.0106$) and a significant time × treatment interaction ($F_{16,185} = 3.80$, $p < 0.0001$). Post hoc analysis revealed that the three BC preparations improved stepping activity at the contralateral paw although with different efficacies and time-courses. As shown in the bar test, both free BC and BC–NLC elevated stepping activity at 30 min after administration (both ∼190% of control). However, the effect of free BC vanished after 3 h (∼125%) whereas that of BC–NLC was significant both at 3 h (∼165%) and 5 h (∼205%) after administration. At 8 h after administration, rats treated with BC–NLC still showed an elevated stepping activity (∼160%), although this value did not reach the level of statistical significance. At variance with the bar test, BC–MAD was able to attenuate motor disability in the drag test, causing a mild elevation at 3 h (∼131%) and 5 h (∼132%) from administration.

Also stepping activity at the ipsilateral paw was affected by BC treatment (Fig 5B). Repeated measure ANOVA on the number of

steps at the ipsilateral paw did not reveal main effect of treatment ($F_{4,36} = 0.96$, $p = 0.44$) but a significant effect of time ($F_{4,185} = 9.82$, $p < 0.0001$) and a time × treatment interaction ($F_{16,185} = 3.43$, $p < 0.0001$). Post hoc analysis showed that among the different BC formulations, only free BC improved stepping activity at the ipsilateral paw, specifically at 30 min after administration (~139%).

Among the various therapeutic applications of BC, we chose to focus on the antiparkinsonian activity since great therapeutic value has been attributed to formulations capable to provide continuous DA receptor stimulation [45,46]. Indeed, it has been demonstrated that long-term side-effects of L-DOPA (mainly dyskinesia) arise from non-physiological "pulsatile" stimulation of DA receptors, which parallels plasmatic drug levels [47]. Thus, continuous delivery or sustained release formulations of L-DOPA have been proved to be less dyskinesiogenic than conventional formulations. Consistently, DA receptor agonists (the most effective alternative to L-DOPA) are less dyskinesiogenic than L-DOPA, probably due to the longer half-life. Achieving a stable and prolonged DA receptor stimulation may also be advantageous in the case of DA agonists, as it allows for a reduction in the frequency of administration and occurrence of side-effects at peak levels. In the present study, we employed two different behavioral tests providing complementary information on motor function: the bar and the drag tests. The responses to BC and its NLC formulation were consistent in both tests. Thus, BC caused a reduction in immobility time (i.e., reduced akinesia) and improvement of stepping activity (i.e., reduced akinesia/bradykinesia), which lasted for at least 90 min and disappeared after 3 h from administration. BC encapsulated in NLC essentially mimicked these effects providing a more prolonged attenuation of motor disability which lasted for at least 5 h and vanished within 8 h. The obtained results extend our previous finding [20] and confirm the ability of BC–NLC to provide longer lasting therapeutic benefit compared to conventional BC formulations. The finding that free BC caused a rapid and transient (30 min) elevation of stepping also at the ipsilateral paw may reflect differences in drugs kinetics since it was not replicated by BC–NLC. In fact, in keeping with the view that conventional BC preparations result in higher peak levels, BC might also improve motility at the ipsilateral paw, which is controlled by the undenervated striatum.

Quite remarkably, BC–MAD was ineffective in the bar test and caused only a mild and delayed elevation of stepping activity in the drag test.

The different in vivo efficacies of BC–MAD and BC–NLC could be attributed to differences in nanoparticulate morphology. In fact, the former are characterized by the coexistence of cubosomes and vesicles while the latter are solid matrix systems.

It has been demonstrated that the intraperitoneal administration prolongs the blood circulation of colloidal drug carriers with respect to the intravenous administration, due to slow absorption of the carrier from the abdominal cavity [48]. On the other hand, it is known that colloidal drug carriers are rapidly opsonized and cleared by the macrophages of the reticulo-endothelial system (RES). Thus, as a general rule, nanosystems are mostly taken up by the liver and the spleen within minutes after systemic administration [49]. In the case of BC–MAD, it can be hypothesized that cubosomes are mainly sequestered by the peritoneal and RES macrophages, as shown for liposomes and nanoparticles [50,51]. Therefore, the mild and sustained effect of BC–MAD may be due to the smaller vesicular liquid-like component of MAD that is responsible for prolonging the half-life of the incorporated drug, having a long circulating time.

Conversely, the NLC structure allows to provide therapeutic BC concentrations to the brain for a long period of time [20]. This might be related to the ability of NLC to pass the BBB [14,18] and/or to a longer stability of NLC in the blood. In fact, previous studies [52] demonstrated that after intraperitoneal administration, nanoparticles show a biphasic absorption: an initial rapid distribution into blood, followed by a slow disposition from peritoneum, resulting in sustained drug release.

Moreover, NLC produced in the presence of poloxamer 188 in the aqueous phase may behave as "stealth carriers," thus being somewhat protected by opsonization [19].

4. Conclusions

This study indicates that both MAD and NLC are able to encapsulate BC, the drug being fully dissolved in nanoparticles. X-ray diffraction and cryo-TEM studies consistently revealed the presence of dispersed cubic phase of *Pn3m* and *Im3m* symmetry in MAD and a gel state with an inner lamellar order in NLC. In vivo studies showed that only BC–NLC were able to markedly attenuate motor deficit in 6-OHDA hemilesioned rats, suggesting that NLC represent a more effective carrier to prolong the half-life of BC in vivo.

Appendix A. Supplementary data

Supplementary data associated with this article can be found, in the online version, at doi:10.1016/j.ejpb.2011.10.015.

References

[1] A. Yaghmur, O. Glatter, Characterization and potential applications of nanostructured aqueous dispersions, Adv. Coll. Interf. Sci. 148 (2009) 333–342.
[2] K. Westesen, B. Siekmann, Biodegradable colloidal drug carrier systems based on solid lipids, in: S. Benita (Ed.), Microencapsulation, Marcel Dekker, New York, 1996, pp. 213–258.
[3] R.H. Muller, K. Mader, S. Gohla, Solid lipid nanoparticles (SLN) for controlled delivery – a review of the state of the art, Eur. J. Pharm. Biopharm. 50 (2000) 161–177.
[4] J. Pardeike, A. Hommoss, R.H. Müller, Lipid nanoparticles (SLN,NLC) in cosmetic and pharmaceutical dermal products, Int. J. Pharm. 366 (2009) 170–184.
[5] R.H. Muller, M. Radtke, S.A. Wissing, Solid lipid nanoparticles (SLN) and nanostructured lipid carriers (NLC) in cosmetic and dermatological preparations, Adv. Drug Del. Rev. 54 (2002) S131s–S155.
[6] J. Gustafsson, H. Ljusberg-Wharen, M. Almgrem, K. Larsson, Cubic lipid/water phase dispersed into submicron particles, Langmuir 12 (1996) 4611–4613.
[7] L. de campo, A. Yaghmur, L. Sagalowicz, M.E. Leser, H. Watzke, O. Gattler, Reversible phase transitions in emulsified nanostructured lipid systems, Langmuir 20 (2004) 5254–5261.
[8] J. Gustafsson, H. Ljusberg-Wharen, M. Almgrem, K. Larsson, Submicron particles of reversed lipid phases in water stabilized by a nonionic amphiphilic polymer, Langmuir 13 (1997) 6964–6971.
[9] E. Esposito, N. Eblovi, S. Rasi, M. Drechsler, G.M. Di Gregorio, E. Menegatti, R. Cortesi, Lipid based supramolecular systems for topical application: a preformulatory study, AAPS Pharm. Sci. 5 (2003) 4 (article 30).
[10] P.T. Spicer, K.L. Hayden, Novel process for producing cubic liquid crystalline nanoparticles (cubosomes), Langmuir 17 (2001) 5748–5756.
[11] M. Nakano, A. Sugita, H. Matsuoka, T. Handa, Small angle X-ray scattering and 13C NMR investigation on the internal structure of cubosome, Langmuir 17 (2001) 3917–3922.
[12] L. Sagalowicz, R. Mezzenga, M.E. Leser, Investigating reversed liquid crystalline mesophases, Curr. Opin. Colloid Interf. Sci. 11 (2006) 224–229.
[13] J. Lai, J. Chen, Y. Lu, J. Sun, F. Hu, Z. Yin, W. Wu, Glyceryl monooleate/Poloxamer 407 cubic nanoparticles as oral drug delivery systems: I. In vitro evaluation and enhanced oral bioavailability of the poorly water-soluble drug simvastatin, AAPS Pharm. Sci. Technol. 10 (2009) 960–966.
[14] E. Barbu, É. Molnàr, J. Tsibouklis, D.C. Górecki, The potential for nanoparticle-based drug delivery to the brain: overcoming the blood–brain barrier, Expert Opin. Drug Del. 6 (2009) 553–565.
[15] S. Pasha, K. Gupta, Various drug delivery approaches to the central nervous system, Expert Opin. Drug Del. 7 (2010) 113–135.
[16] V. Kabanov, E.V. Batrakova, New technologies for drug delivery across the blood brain barrier, Curr. Pharm. Des. 10 (2004) 1355–1363.
[17] K. Andrieux, P. Couvreur, Polyalkylcyanoacrylate nanoparticles for delivery of drugs across the blood–brain barrier, Nanomed. Nanobiotechnol. 1 (2009) 463–474.
[18] I.P. Kaur, R. Bhandari, S. Bhandari, V. Kakkar, Potential of solid lipid nanoparticles in brain targeting, J. Control. Rel. 127 (2008) 97–109.
[19] M.D. Joshi, R.H. Müller, Lipid nanoparticles for parenteral delivery of actives, Eur. J. Pharm. Biopharm. 71 (2009) 161–172.
[20] E. Esposito, M. Fantin, M. Marti, M. Drechsler, L. Paccamiccio, P. Mariani, E. Sivieri, F. Lain, E. Menegatti, M. Morari, R. Cortesi, Solid lipid nanoparticles as delivery systems for bromocriptine, Pharm. Res. 25 (2008) 1521–1530.

[21] http://www.fscimage.fishersci.com/msds/06352.html.
[22] E. Esposito, R. Cortesi, M. Drechsler, L. Paccamiccio, P. Mariani, C. Contado, E. Stellin, E. Menegatti, F. Bonina, C. Puglia, Cubosome dispersions as delivery systems for percutaneous administration of indomethacin, Pharm. Res. 22 (2005) 2163–2173.
[23] R. Pecora, Dynamic light scattering measurement of nanometer particles in liquids, J. Nanoparticle Res. 2 (2000) 123–131.
[24] C. Contado, A. Dalpiaz, E. Leo, M. Zborowski, P.S. Williams, Complementary use of flow and sedimentation field-flow fractionation techniques for size characterizing biodegradable poly(lactic acid) nanospheres, J. Chromatogr. A 1157 (2007) 321–335.
[25] C. Contado, G. Blo, F. Fagioli, F. Dondi, R. Beckett, Characterisation of River Po particles by sedimentation field-flow fractionation coupled to GFAAS and ICP-MS, Colloid Surf. A – Physicochem. Eng. Asp. 120 (1997) 47–59.
[26] P. Andreozzi, S.S. Funari, C. La Mesa, P. Mariani, M.G. Ortore, R. Sinibaldi, F. Spinozzi, Multi- to unilamellar transitions in catanionic vesicles, J. Phys. Chem. B 114 (2010) 8056–8060.
[27] P. Mariani, V. Luzzati, H. Delacroix, Cubic phases of lipid containing systems. Structure analysis and biological implications, J. Mol. Biol. 204 (1988) 165–189.
[28] F. Spinozzi, L. Paccamiccio, P. Mariani, L.Q. Amaral, Melting regime of the anionic phospholipid DMPG: new lamellar phase and porous bilayer model, Langmuir 26 (2010) 6484–6493.
[29] M. Marti, F. Mela, M. Fantin, S. Zucchini, J. M Brown, J. Witta, M. Di Benedetto, B. Buzas, R.K. Reinscheid, S. Salvadori, R. Guerrini, P. Romualdi, S. Candeletti, M. Simonato, B.M. Cox, M. Morari, Blockade of nociceptin/orphanin FQ transmission attenuates symptoms and neurodegeneration associated with Parkinson's disease, J. Neurosci. 95 (2005) 9591–9601.
[30] G. Paxinos, C. Watson, The rat brain in stereotaxic coordinates, Academic, Sydney, 1982.
[31] M. Marti, C. Trapella, R. Viaro, M. Morari, The nociceptin/orphanin FQ receptor antagonist J-113397 and L-DOPA additively attenuate experimental parkinsonism through overinhibition of the nigrothalamic pathway, J. Neurosci. 27 (2007) 1297–1307.
[32] M. Marti, F. Mela, C. Bianchi, L. Beani, M. Morari, Striatal dopamine-NMDA receptor interactions in the modulation of glutamate release in the substantia nigra pars reticulata in vivo. Opposite role for D1 and D2 receptors, J. Neurochem. 83 (2002) 635–644.
[33] P.R. Sanberg, M.D. Bunsey, M. Giordano, A.B. Norman, The catalepsy test: its ups and downs, Behav. Neurosci. 102 (1988) 748–759.
[34] T. Schallert, M. De Rick, I.Q. Whishaw, V.D. Ramirez, P. Teitelbaum, Excessive bracing reactions and their control by atropine and L-DOPA in an animal analog of Parkinsonism, Exp. Neurol. 64 (1979) 33–43.
[35] C. Nastruzzi, C. Pastesini, R. Cortesi, E. Esposito, R. Gambari, E. Menegatti, Kinetic of bromocriptine release from microspheres: comparative analysis between different in vitro models, J. Microencapsul. 11 (1993) 565–574.
[36] E. Esposito, R. Cortesi, E. Menegatti, C. Nastruzzi, Preformed gelatin microspheres as a delivery system for bromocriptine, Pharm. Sci. Comm. 4 (1994) 239–246.
[37] R. Mahajan, Bromocriptine mesylate: FDA-approved novel treatment for type-2 diabetes, Indian J. Pharmacol. 41 (2009) 197–198.
[38] G. Garg, S. Saraf, S. Saraf, Cubosomes: an overview, Biol. Pharm. Bull. 30 (2007) 350–353.
[39] J.C. Shah, Y. Sadhale, D.M. Chilukuri, Cubic phase gels as drug delivery systems, Adv. Drug Deliv. Rev. 47 (2001) 229–250.
[40] K. Jores, W. Mehnert, M. Drechsler, H. Bunjes, C. Johann, K. Maeder, Investigations on the structure of solid lipid nanoparticles (SLN) and oil-loaded solid lipid nanoparticles by photon correlation spectroscopy, field-flow fractionation and transmission electron microscopy, J. Control. Rel. 95 (2004) 217–227.
[41] G. Worle, M. Drechsler, M.H.J. Koch, B. Siekmann, K. Westesen, H. Bunjes, Influence of composition and preparation parameters on the properties of aqueous Monoolein dispersions, Int. J. Pharm. 329 (2007) 150–157.
[42] V. Luzzati, H. Delacroix, A. Gulik, T. Gulik-Krzywicki, P. Mariani, R. Vargas, The cubic phases of lipids, Curr. Top. Membr. 44 (1997) 3–24.
[43] M. Pisani, S. Bernstorff, C. Ferrero, P. Mariani, Pressure induced cubic-to-cubic phase transition in Monoolein hydrated system, J. Phys. Chem. B 105 (2001) 3109–3119.
[44] A. Yaghmur, L. de Campo, S. Salentinig, L. Sagalowicz, M.E. Leser, O. Glatter, Oil-loaded monolinolein-based particles with confined inverse discontinuous cubic structure (Fd3m), Langmuir 22 (2006) 517–521.
[45] A. Di Stefano, P. Sozio, A. Iannitelli, L.S. Cerasa, New drug delivery strategies for improved Parkinson's disease therapy, Expert Opin. Drug Del. 6 (2009) 389–404.
[46] G. Modi, V. Pillay, Y.E. Choonara, V.M. Ndesendo, L.C. du Toit, D. Naidoo, Nanotechnological applications for the treatment of neurodegenerative disorders, Prog. Neurobiol. 88 (2009) 272–285.
[47] J.A. Obeso, F. Grandas, M.T. Herrero, R. Horowski, The role of pulsatile versus continuous dopamine receptor stimulation for functional recovery in Parkinson's disease, Eur. J. Neurosci. 6 (1994) 889–897.
[48] Y. Sadzuka, R. Hirama, T. Sonobe, Effects of intraperitoneal administration of liposomes and methods of preparing liposomes for local therapy, Toxicol. Lett. 126 (2002) 83–90.
[49] J.K. Vasir, M.K. Reddy, V.D. Labhasetwar, Nanosystems in drug targeting: opportunities and challenges, Curr. Nanosci. 1 (2005) 47–64.
[50] T.M. Allen, C.B. Hansen, L.S.S. Guo, Subcutaneous administration of liposomes: a comparison with the intravenous and intraperitoneal routes of injection, Biochim. Biophys. Acta 1150 (1993) 9–169.
[51] L.H. Reddy, R.K. Sharma, K. Chuttani, A.K. Mishra, R.S.R. Murthy, Influence of administration route on tumour uptake and biodistribution of etoposide loaded solid lipid nanoparticles in Dalton's lymphoma tumour bearing mice, J. Control. Rel. 105 (2005) 185–198.
[52] L.H. Reddy, R.S.R. Murthy, Pharmacokinetics and biodistribution studies of doxorubicin loaded poly(butyl cyanoacrilate) nanoparticles synthesized by two different techniques, Biomed. Papers 148 (2) (2004) 161–166.